High-Performance Balun for a Dual-Polarized Dipole Antenna

High-Performance Balun for a Dual-Polarized Dipole Antenna

Grzegorz Wolosinski [1*], Vincent Fusco [1], Pawel Rulikowski [2]

[1] Institute of Electronics, Communications and Information Technology (ECIT), Queens University of Belfast, Belfast, United Kingdom.
[2] RF Access Group, Nokia Bell Labs, Dublin, Ireland.
[*] gwolosinski01@qub.ac.uk

Abstract: This paper proposes a detailed analysis on the operation of a high-performance balun for a dual-polarized dipole antenna. The main feature of this balun is to transform a coaxial feed into a differential feed which can enable very high performance for dual-polarized configurations. First, we identify the key factors that allow the new balun to achieve better differential properties respect to the feeding approach typically found in the literature. Second, we investigate the balun properties and the achievable antenna performance with extensive simulations. Next, we prototype and measure the antenna proving that very high port-to-port isolation and low cross-polarization level (XPL) can be achieved over a broadband operation by means of this balun. Finally, we further investigate the operation of the balun through its physical decomposition revealing the minimum requirement to achieve high port-to-port isolation in dual-polarized dipole antennas.

1. Introduction

The increasing demand for wireless communication services has recently led to the extension of the available spectrum and the need to deploy a growing number of base stations with reduced size. These requirements have driven the wireless research community to focus on co-located dual-polarized antennas with low cross-polarization level (XPL) and high port-to-port isolation (i.e. $-|S_{12}|$ in dB) over a prescribed broadband operation. In fact, the XPL and S_{12} are key parameters for evaluating dual-polarized antennas as they represent the unwanted power leakage among the two polarization states respectively in the far field and at the circuit ports. Typically, dual-polarized antennas for base station applications consist of two reflector-backed crossed dipoles fed by means of a pair of coaxial cables attached at right angle [1]-[9]. Although the unbalanced nature of the coaxial feed can limit the antenna performance, this feeding approach has obtained great popularity due to its ease of implementation. In order to improve the differential properties of coaxial-based feeds the use of balun structures has been proposed in [10]-[12]. Despite this strategy, the reported improvements in terms of XPL and S_{12} are marginal or none if compared to similar antennas without balun, e.g. [1]-[9]. Indeed, in the authors' opinion, the main aspect that limits the XPL and S_{12} of current dual-polarized dipole antennas has not been fully identified and addressed in the literature. In this regard, the authors have recently proposed a dual-polarized antenna based on a new balun which can enable very high antenna performance over a broadband operation [13]. This paper extends the work in [13] with a detailed analysis on the operation of the proposed balun and its effect on antenna performance. Section 2 proposes the main idea behind the new balun. Section 3 reports the antenna structure and the operation of the balun. Section 4 evaluates the differential properties of the balun and the achievable antenna performance. Section 5 reports the manufacturing process and measurements of the prototyped antenna. Finally, Section 6 further investigates the operation of the balun through its physical decomposition.

2. Feeding Arrangement

Directional dual-polarized dipole antennas are typically fed with coaxial cables which are passed through the ground plane or reflector and attached at right angle to the dipoles [1]-[12]. This approach normally requires a crossover connector between each feed cable and its dipole resulting in a feeding section with at least one right-angle transition (or discontinuity) as shown in Fig. 1 (a). A typical associated current distribution at the feeding section is schematized in Fig. 1 (a). This shows that such a discontinuity can radiate and couple unwanted energy to the orthogonal dipole potentially degrading the required differential property of the feed and in turn the XPL and S_{12} of the antenna. In the following we refer to this feeding arrangement as the classical approach. To minimise this effect, in [13] we proposed a dual-polarized dipole antenna whose feeding section to one dipole is schematized in Fig. 1 (b). This new arrangement provides beneficial aspects to the feeding section respect to the classical approach. First, the need for a crossover connector is removed since the inner conductor of the feed cable is used for this purpose. Second and most relevant, the absence of a right-angle transition limits the effect of the discontinuity between the feed cable and its dipole therefore establishing favourable conditions to achieve a balanced feed. In general, the remaining part of the feed cable (between the dipole and its reflector) can affect the symmetry of the current distribution on the antenna thus its performance. Therefore, symmetric dummy structures should be employed to restore the physical symmetry of the antenna.

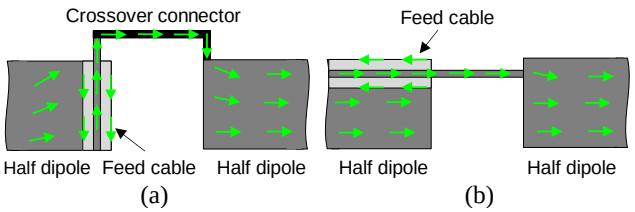

Fig. 1. *Cross-sectional view of the schematic feeding section with current distribution upon coaxial feed excitation.*
(a) Classical and **(b)** proposed approach.

3. Antenna Structure and Balun Operation

The broadband dual-polarized dipole antenna presented in [13] is shown in Fig. 2 (a). The antenna consists of two reflector-backed crossed dipoles which are driven by a pair of coaxial ports. The novelty of the antenna relies on the feeding arrangement introduced in Fig. 1 (b) rather than on the radiating elements whose basic shape, inspired from [4], was selected to achieve broadband input impedance matching. The cross-section of the antenna highlights the feeding structure of one dipole as shown in Fig. 2 (b). This consists of a coaxial cable and a symmetric dummy cable attached to the dipole along its longitudinal axis which are symmetrically bent toward the reflector and short-circuited to the latter. The two conductors being a mirror copy of each other establish a highly balanced transmission line short-circuited at one end and connected in parallel to the dipole at the other end. The overall structure acts as a balun between the feed port and the feeding section of the dipole.

The orthogonal dipole of the antenna is fed by an identical balun whose only difference is a relative shift of 1.3 mm along z-axis to avoid cable overlap. The distance between the dipoles and the reflector is a quarter wavelength at the centre operating frequency, i.e. 2.35 GHz, thus at this frequency each balun provides approximately an open circuit in parallel to its dipole. For other operating frequencies within bandwidth, i.e. 1.7-3 GHz, each balun provides a reactance instead of an open circuit as per the transmission line theory. Regardless of the provided impedance, the high symmetry of the balun allows to achieve high differential properties in a broadband operation.

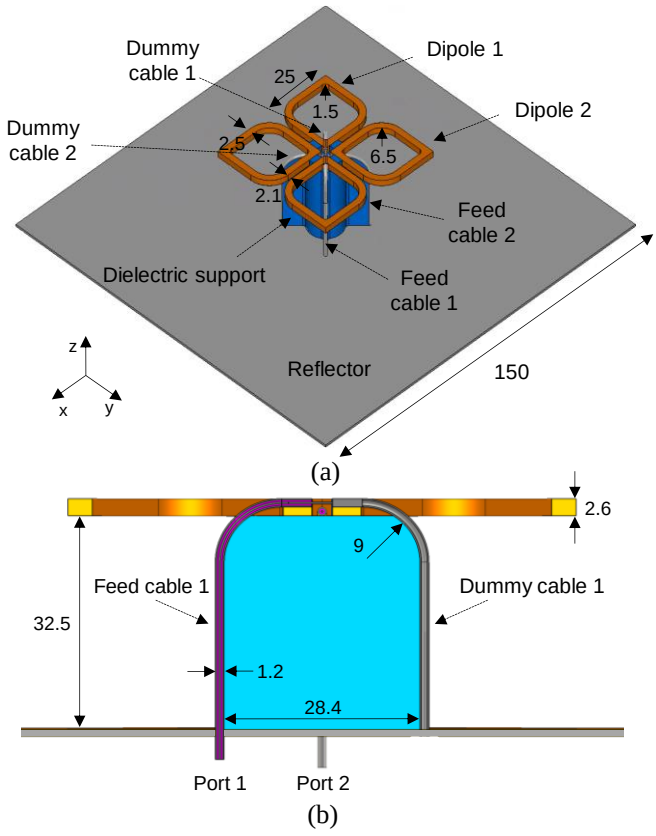

Fig. 2. *Proposed antenna with reported dimensions in mm.* **(a)** Isometric and **(b)** cross-sectional view along dipole 1.

4. Differential Properties

This section quantitatively evaluates the differential properties of the balun and the achievable XPL and S_{12} of the antenna. The following simulations are obtained with the use of a commercial electromagnetic software [14]. A probe is placed between the end of each cable and the reflector in order to sample the current onto the outer conductors of the four cables. The antenna is fed at port 1 while port 2 is terminated with 50 Ω. The peak value of the magnitude normalized to the excitation port and the relative phase on each probe are reported in Fig. 3. The currents on feed and dummy cable 1 are equal in magnitude and 180° out of phase over the entire bandwidth, which confirm the high differential properties of the balun. Moreover, the magnitude of these currents shows a minimum at 2.35 GHz confirming the quarter-wave transformer functioning of the balun at its centre operating frequency. The currents on feed and dummy cable 2 are equal in magnitude with a peak value lower than 40 dB respect to the first pair of cables and result mainly in phase. This result shows that the two balun structures are highly isolated between each other. In the following the XPL at boresight and the maximum XPL evaluated within the angular region [−60, 60]° are considered and referred to as XPL and $\overline{\text{XPL}}$, respectively. The simulated XPL, maximum $\overline{\text{XPL}}$ along E and H-plane, and S_{12} of the antenna with and without dummy cables are reported in Fig. 4.

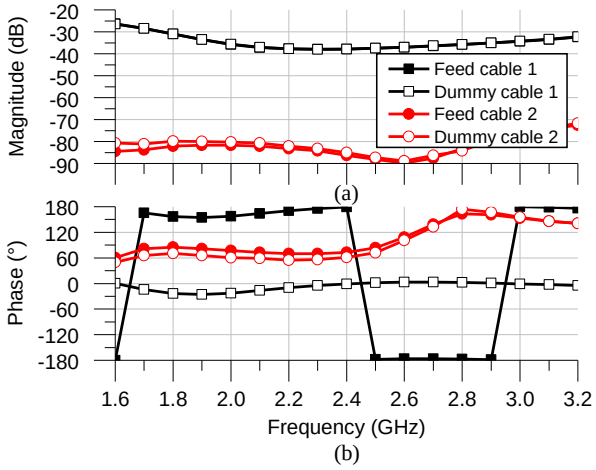

Fig. 3. *Probe current normalised to the excitation port.* **(a)** Peak value of the magnitude and **(b)** relative phase.

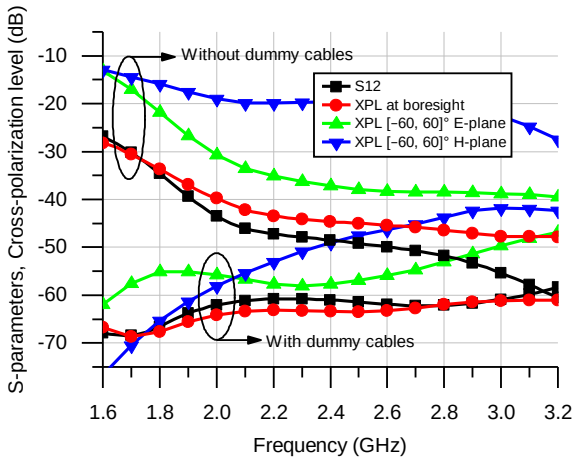

Fig. 4. *Simulated S_{12}, XPL at boresight, and maximum XPL within the angular region [−60, 60]° along E and H-plane.*

As a result of the highly symmetrical current distribution the complete antenna shows XPL and S_{12} as low as −60 dB over the entire bandwidth while the $\overline{XPL}$ evaluated along E and H-plane is always maintained below −41 dB. Instead, the antenna without dummy cables exhibits significant performance degradation concerning all the studied parameters especially at the lower end of the band due to high asymmetries in the current distribution.

5. Antenna Prototype

5.1. Manufacturing Process

The studied antenna has been prototyped as shown in Fig. 5. The radiating elements were made of brass while the reflector was realized using a double-sided copper FR-4 board. The dielectric support was 3D printed in polylactic acid with 80% filling factor. Each balun was realized by employing a single chunk of a 50-Ω semi-rigid coaxial cable with 1.2 mm of outer diameter. First, each cable was soldered to two radiating elements after part of its outer conductor and dielectric material were removed to obtain the feeding section (see bottom left inset in Fig. 5). Second, the inner and outer conductor of each cable were short circuited at an arbitrary side of the feeding section to obtain a dummy cable. Next, the resulting cables were passed through four holes in the reflector and soldered front and back to establish electrical connection and facilitate mechanical stability (see bottom right inset in Fig. 5). Epoxy glue was used during the assembly to fix the radiating elements to the dielectric support and the latter to the reflector. Finally, two SMA connectors were applied to the feed cables to obtain accessible antenna ports.

5.2. Measurements

The S-parameters of the antenna has been measured with a Rohde & Schwarz ZVA40 Vector Network Analyser. The measured results show good agreement with simulations as reported in Fig. 6. For a return loss (RL) ≥ 12.8 dB the operating band of the antenna is 1.68-3.04 GHz, which results in 58% of bandwidth. The measured S_{12} is higher than in simulation, however its level is maintained below −49 dB over the entire bandwidth. The antenna has been characterized within a reverberation chamber to obtain the total radiation efficiency and correlation coefficient as reported in Fig. 7 (a)-(b), respectively. The measurement setup features a standard deviation uncertainty better than 0.5 dB (12% in linear scale), e.g. see [15]. The measured total radiation efficiency at both antenna ports show good agreement with simulations featuring values better than 85% (−0.7 dB) within the operating bandwidth. The measured correlation coefficient between the two antenna ports is better than 0.34 while the simulated one is of the order of 10^{-4} and therefore is not reported for scaling reason. This discrepancy is mainly attributed to the directional features of the measured antenna which reduces the accuracy of obtaining a rich isotropic multipath environment within the reverberation chamber setup, e.g. see [15]. The radiation patterns of the antenna have been characterized in far-field antenna range within an anechoic chamber. The E and H-plane of dipole 1 at 1.8, 2.2, and 2.7 GHz are reported in Fig. 8-10 (a)-(b), respectively. The radiation patterns of dipole 2 show high similarity and are not reported for brevity. The measured and simulated co-polar components show very good agreement while the measured cross-polar components show a general higher level respect to the simulated ones. Such a disagreement can be due to slight misalignments in the measurements campaign, finite XPL of the reference antenna,

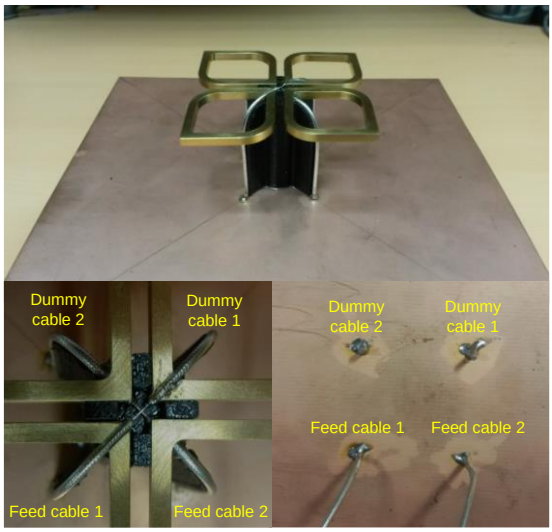

Fig. 5. *Photograph of the prototyped antenna. Bottom left inset shows details of the feeding section. Bottom right inset shows back of the antenna. Labels highlight the arrangement of the cables.*

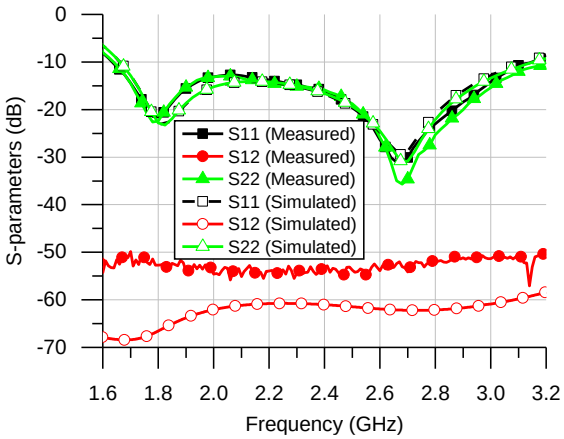

Fig. 6. *S-parameters of the antenna.*

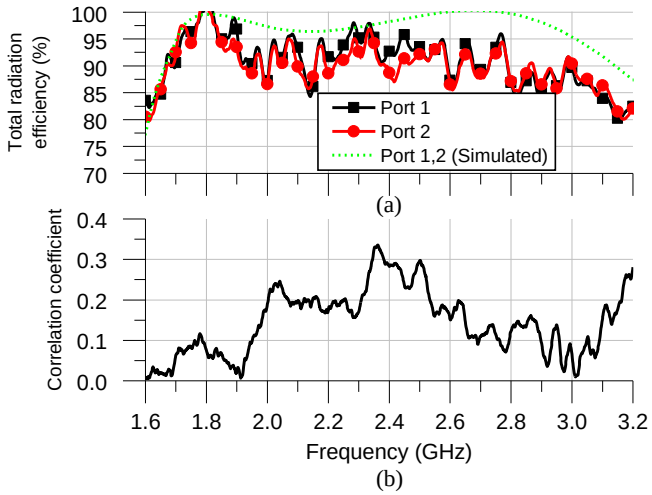

Fig. 7. **(a)** Measured and simulated total radiation efficiency **(b)** measured correlation coefficient.

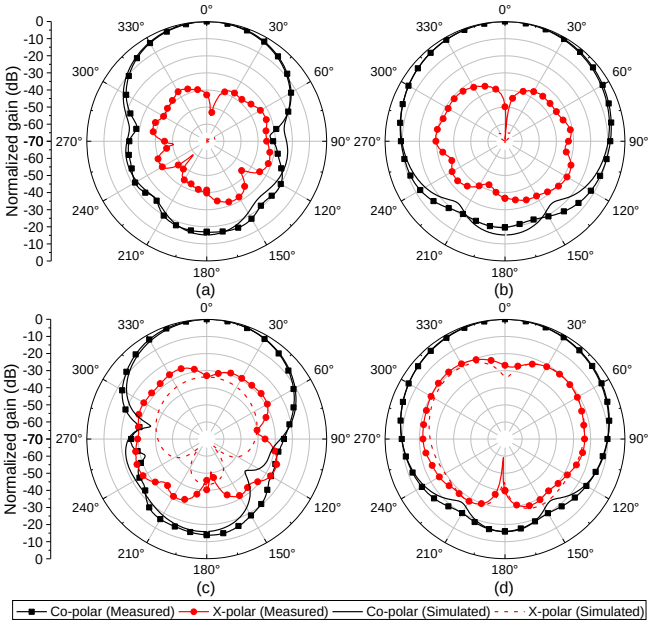

Fig. 8. *Radiation patterns of dipole 1 at 1.8 GHz.*
(a) E-plane and **(b)** H-plane with dummy cable 1.
(c) E-plane and **(d)** H-plane without dummy cable 1.

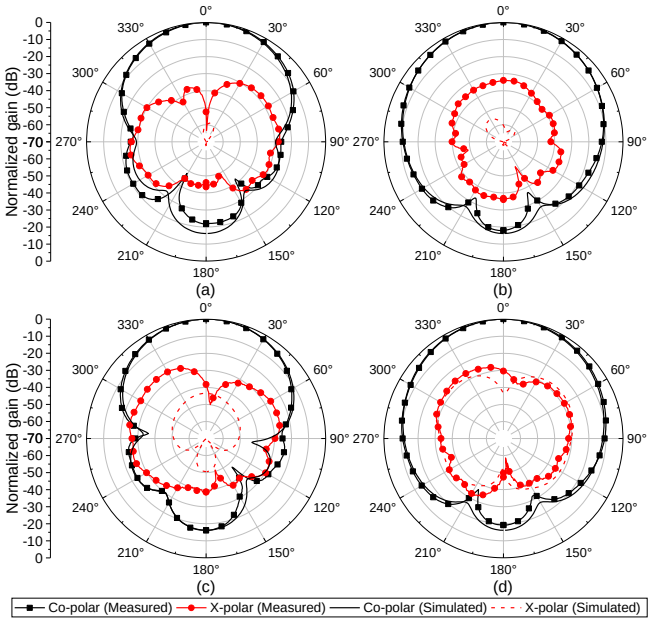

Fig. 9. *Radiation patterns of dipole 1 at 2.2 GHz.*
(a) E-plane and **(b)** H-plane with dummy cable 1.
(c) E-plane and **(d)** H-plane without dummy cable 1.

and to non-ideal prototyping. Nevertheless, the XPL and $\overline{\text{XPL}}$ along E and H-plane are maintained respectively below −34 and −16 dB for the reported frequencies. For the purpose of comparison, the maximum XPL, $\overline{\text{XPL}}$ along E and H-plane, and S_{12} achieved in this work and in [1]-[12] are reported in Table I. The antenna in this work shows an improvement in the XPL, $\overline{\text{XPL}}$, and S_{12} respectively of 2, 6, and 14 dB with respect to the overall best performance achieved in the reported references. As far as other antenna parameters are concerned the gain at boresight is 8.9 dB ± 0.3 dB while the front-to-back ratio (F/B) is 16.6 dB ± 1.4 dB whose relatively large value is due to the electrically small size and flat shape of the reflector. The half power beamwidth (HPBW) along E

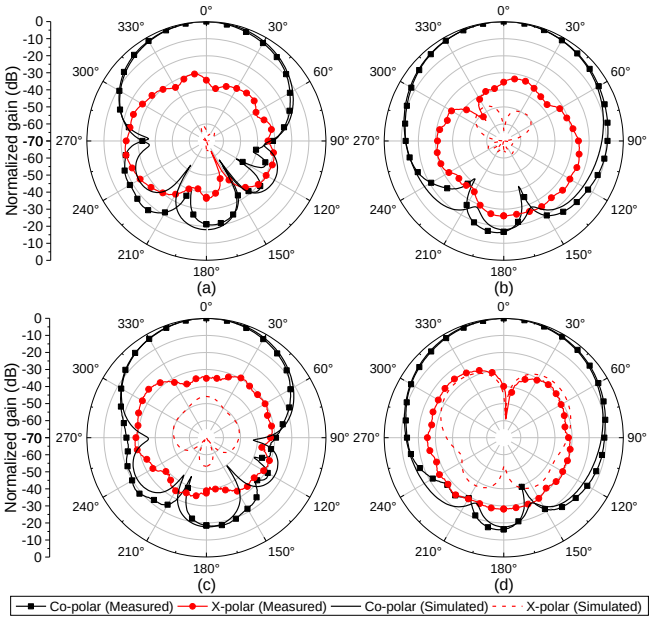

Fig. 10. *Radiation patterns of dipole 1 at 2.7 GHz.*
(a) E-plane and **(b)** H-plane with dummy cable 1.
(c) E-plane and **(d)** H-plane without dummy cable 1.

and H-plane is respectively 59° ± 1° and 85.5° ± 10.5° whose large difference is due to the intrinsic radiation characteristics of a dipole antenna placed above a planar reflector. It is worth noting that to improve the F/B and equalize the HPBW along E and H-plane [16], further optimization of the shape of the reflector would be required.

6. Balun Decomposition

This section further investigates the operation of the balun through its physical decomposition. The dummy cables were systematically removed from the antenna and S-parameters with radiation patterns were measured for each situation. The S_{11} and S_{12} are reported in Fig. 11. The removal of dummy cable 1 changes the input matching of dipole 1 although with a limited impact as expected by the operation of the balun as a short-circuited quarter-wave impedance transformer. The input matching of dipole 2 remains unchanged. Even though the differential feed of one dipole is compromised the S_{12} of the antenna is mainly unaffected. Such a result can be explained by considering a

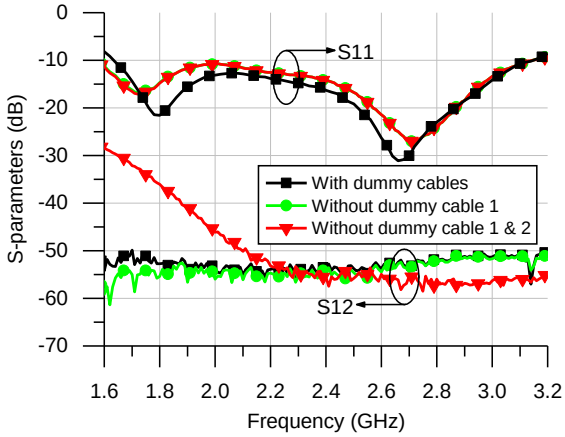

Fig. 11. *Measured S_{11} and S_{12} of the prototype antenna.*

Table 1 Maximum value of XPL, $\overline{\text{XPL}}$ along E and H-plane, and S_{12} within bandwidth (BW). NG: Not Given.

Reference	Balun	BW (%), RL (dB)	XPL (dB)	$\overline{\text{XPL}}$ (dB)	S_{12} (dB)
[1]	No	45 (RL ≥ 9.5)	−28	NG	−31
[2]	No	45 (RL ≥ 14)	NG	NG	−25
[3]	No	45 (RL ≥ 14)	−20	NG	−30
[4]	No	57 (RL ≥ 14)	−24	NG	−31
[5]	No	51 (RL ≥ 15.5)	NG	NG	−27
[6]	No	30 (RL ≥ 14)	−16	−10	−25
[7]	No	40 (RL ≥ 15)	NG	NG	−32
[8]	No	22 (RL ≥ 10)	−18	NG	−28
[9]	No	8.2 (RL ≥ 15.5)	−29	NG	−35
[10]	Yes	56 (RL ≥ 14)	−21	NG	−25
[11]	Yes	45 (RL ≥ 14)	−21	−10	−25
[12]	Yes	45 (RL ≥ 15.5)	−32	NG	−32
This work	Yes	58 (RL ≥ 12.8)	−34	−16	−49

Table 2 Measured radiation parameters of dipole 1.

Parameter	With dummy cable 1			Without dummy cable 1		
Frequency (GHz)	1.8	2.2	2.7	1.8	2.2	2.7
Gain (dB)	8.6	9.2	8.9	8.5	9.2	8.9
F/B (dB)	15.3	16.2	18	15.9	16.2	17.7
XPL E-plane (dB)	−43	−53	−34	−33	−38	−35
XPL H-plane (dB)	−50	−34	−36	−27	−31	−40
$\overline{\text{XPL}}$ E-plane (dB)	−21	−17	−16	−15	−14	−14
$\overline{\text{XPL}}$ H-plane (dB)	−27	−31	−26	−15	−20	−18
HPBW E-plane (°)	58	60	60	64	62	57
HPBW H-plane (°)	96	75	77	86	76	75

general dual-polarized dipole antenna whose first and second element are respectively driven by a non-ideal and ideal differential feed. Without loss of generality let us feed the first dipole and terminate the second one on its reference impedance. It turns out that the asymmetric current excited onto the first dipole induces symmetric currents onto both arms of the second dipole regardless of the degree of the asymmetry. This, in turn, results in a net current at the port of the second dipole equal to zero, providing $|S_{12}| = 0$ as in the case of ideal differential feeds at both dipoles. This result shows that the necessary and sufficient condition to achieve $|S_{12}| = 0$ in a co-located dual-polarized dipole antenna is the employment of only one differential feed within the antenna. Moreover, the above fact suggests that $|S_{12}|$ has a lower bound established by the best differential performance among the two feeds. The measured radiation patterns of dipole 1 without its dummy cable are reported in Fig. 8-10 (c)-(d). The co-polar components result squinted along E-plane and the level of cross-polar components is compromised respect to the complete antenna. These effects are more pronounced at lower operating frequencies as the degree of asymmetry in the current distribution is higher. The radiation patterns of dipole 2 remain mainly unchanged. The radiation parameters of dipole 1 with and without its dummy cable are summarized in Table II. The absence of the dummy cable has very little impact on antenna gain and F/B while the maximum XPL and $\overline{\text{XPL}}$ increase to −27 dB and −14 dB, respectively. The HPBW along E and H-plane become respectively 60.5° ± 3.5° and 80.5° ± 5.5°. Finally, the removal of dummy cable 2 from the antenna affects the input matching and the radiation patterns of dipole 2 in the same way as for dipole 1 and also degrades S_{12} at low operating frequencies due to the impairment of the differential properties of both antenna feeds. It is interesting to note that there exists a specific frequency f_s above which the obtained S_{12} slightly outperforms the S_{12} of the complete antenna. This is due to the superposition of two effects that occur on each dipole when both dummy cables are removed. The first one is the current flowing onto the outer conductor of the feed cable which is not balanced by an equal and opposite current. The second effect is the current imbalance between the two halves of each dipole. Full-wave simulations have shown that for specific bending radius of the feed cables and operating frequencies, these two effects can combine in such a way to provide two orthogonal current distributions associated to the antenna ports (even though the physical symmetry is broken), leading to an S_{12} comparable or even lower with respect to the complete antenna. In the measurements f_s = 2.35 GHz while in simulations f_s = 3.15 GHz. This discrepancy is due to the higher measured S_{12} of the complete antenna which causes f_s to be shifted towards lower frequencies. Since the beneficial combination of the above effects only occurs in specific circumstances, this result should be considered as a second-order effect respect to the overall benefits provided by the full feeding structure.

7. Conclusion

In this paper we have investigated the properties of a high-performance balun for a dual-polarized dipole antenna. The proposed arrangement of the feed cable and the deployment of a symmetric dummy cable have shown to operate as a highly differential feed that leads to very high antenna performance. Measurements of the prototyped antenna have proven that $|S_{12}| \leq -49$ dB, XPL ≤ -34 dB, and $\overline{\text{XPL}} \leq -16$ dB along E and H-plane can be achieved over a broadband operation. These results show that the proposed balun is able to provide superior antenna performance respect to the coaxial-based right-angle feeding approach typically found in the literature. Moreover, the physical decomposition of the dummy cables from the antenna has revealed that the necessary and sufficient condition to achieve $|S_{12}| = 0$ in a co-located dual-polarized dipole antenna is to employ only one high-performance differential feed instead of two that are generally thought to be required. This general feature relaxes the requirements for achieving high port-to-port isolation in dual-polarized dipole antennas.

8. Acknowledgments

This work was supported in part by Marie Curie European Industrial Doctorate (EID) programme ARTISAN (grant no. 316426) and Nokia Bell Labs, Ireland.

9. References

1. Lee, H., and Lee, B.: 'Compact broadband dual-polarized antenna for indoor MIMO wireless communication systems', *IEEE Trans. Antennas Propag.*, 2016, **64**, (2), pp. 766–770.
2. Chu, Q.X., Wen D.L., and Luo, Y.: 'A broadband ±45◦ dual-polarized antenna with y-shaped feeding lines', *IEEE Trans. Antennas Propag.*, 2015, **63**, (2), pp. 483–490.
3. Cui, Y., Li, R.L., and Fu, H.: 'A broadband dual-polarized planar antenna for 2g/3g/lte base stations', *IEEE Trans. Antennas Propag.*, 2014, **62**, (9), pp. 4836–4840.
4. Bao, Z., Nie, Z., and Zong, X.: 'A novel broadband dual-polarization antenna utilizing strong mutual coupling', *IEEE Trans. Antennas Propag.*, 2014, **62**, (1), pp. 450–454.
5. Zheng, D. Z., and Chu, Q.X.: 'A multimode wideband ±45° dual-polarized antenna with embedded loops', *IEEE Antennas Wireless Propag. Lett.*, 2017, **16**, pp. 633–636.
6. Wen, D.L., Zheng, D.Z., and Chu, Q.X.: 'A dual-polarized planar antenna using four folded dipoles and its array for base stations', *IEEE Trans. Antennas Propag.*, 2016, **64**, (12), pp. 5536-5542.
7. Cui, Y., Niu, Y., Qi, C., *et al.*: 'A broadband flush-mountable dual-polarized dual-slot antenna', *IEEE Antennas Wireless Propag. Lett.*, 2018, **PP**, (99), pp. 1–1.
8. Zhai, H., Xi, L., Zang, Y., *et al.*: 'A low-profile dual-polarized high-isolation MIMO antenna arrays for wideband base-station applications', *IEEE Trans. Antennas Propag.*, 2018, **66**, (1), pp. 191–202.
9. Duan, W., Zhang, X.Y., Pan,Y.M., *et al.*: 'Dual-polarized filtering antenna with high selectivity and low cross polarization', *IEEE Trans. Antennas Propag.*, 2016, **64**, (10), pp. 4188–4196.
10. Huang, H., Liu, Y., and Gong, S.: 'A broadband dual-polarized base station antenna with anti-interference capability', *IEEE Antennas Wireless Propag. Lett.*, 2017, **16**, pp. 613–616.
11. Luo, Y., Chu, Q.X., and Wen, D.L.: 'A plus/minus 45 degree dual-polarized base-station antenna with enhanced cross-polarization discrimination via addition of four parasitic elements placed in a square contour', *IEEE Trans. Antennas Propag.*, 2016, **64**, (4), pp. 1514–1519.
12. Bao, Z., Nie, Z., and Zong, X.: 'A broadband dual-polarization antenna element for wireless communication base station', *IEEE Asia-Pacific Conf. Antennas Propag.*, Singapore, Singapore, Aug. 2012, pp. 144–146.
13. Wolosinski, G., Fusco, V., and Rulikowski P.: 'Broadband dual-polarized antenna with high port isolation and polarization purity', *IEEE Int. Symp. Antennas Propag. (APSURSI)*, Fajardo, Puerto Rico, June 2016, pp. 1581–1582.
14. CST Microwave Studio® 2016, www.cst.com.
15. Lotback Patane, C.S., Franzen, M., and Orlenius. C.: 'Analysis and improvement of reverberation chamber method for characterization of small and terminal antennas', *Proc. 5th European Conf. Antennas Propag.*, Rome, Italy, Apr. 2011, pp. 1832–1836.
16. Balanis, C.A.. 'Antenna Theory: Analysis and Design' (*John Wiley & Sons, Inc.* Press, New Jersey, 2005, 4th edn.), pp. 875–884.